JACS
JOURNAL OF THE AMERICAN CHEMICAL SOCIETY
Article
pubs.acs.org/JACS

Photooxidation of Ammonia on TiO_2 as a Source of NO and NO_2 under Atmospheric Conditions

Mulu A. Kebede,[†] Mychel E. Varner,[‡] Nicole K. Scharko,[†] R. Benny Gerber,*[,‡,§] and Jonathan D. Raff*[,†]

[†]School of Public and Environmental Affairs and Department of Chemistry, Indiana University, Bloomington, Indiana 47405-2204, United States

[‡]Department of Chemistry, University of California—Irvine, Irvine, California 92697-2025, United States

[§]Department of Physical Chemistry and the Fritz Haber Research Center, The Hebrew University, Jerusalem, Israel 91904

ABSTRACT: Ammonia is the most abundant reduced nitrogen species in the atmosphere and an important precursor in the industrial-scale production of nitric acid. A coated-wall flow tube coupled to a chemiluminescence NO_x analyzer was used to study the kinetics of NH_3 uptake and NO_x formation from photochemistry initiated on irradiated ($\lambda > 290$ nm) TiO_2 surfaces under atmospherically relevant conditions. The speciation of NH_3 on TiO_2 surfaces in the presence of surface-adsorbed water was determined using diffuse reflection infrared Fourier transform spectroscopy. The uptake kinetics exhibit an inverse dependence on NH_3 concentration as expected for reactions proceeding via a Langmuir−Hinshelwood mechanism. The mechanism of NO_x formation is shown to be humidity dependent: Water-catalyzed reactions promote NO_x formation up to a relative humidity of 50%. Less NO_x is formed above 50%, where increasing amounts of adsorbed water may hinder access to reactive sites, promote formation of unreactive NH_4^+, and reduce oxidant levels due to higher OH radical recombination rates. A theoretical study of the reaction between the NH_2 photoproduct and O_2 in the presence of H_2O supports the experimental conclusion that NO_x formation is catalyzed by water. Calculations at the MP2 and CCSD(T) level on the bare $NH_2 + O_2$ reaction and the reaction of $NH_2 + O_2$ in small water clusters were carried out. Solvation of NH_2OO and NHOOH intermediates likely facilitates isomerization via proton transfer along water wires, such that the steps leading ultimately to NO are exothermic. These results show that photooxidation of low levels of NH_3 on TiO_2 surfaces represents a source of atmospheric NO_x, which is a precursor to ozone. The proposed mechanism may be broadly applicable to dissociative chemisorption of NH_3 on other metal oxide surfaces encountered in rural and urban environments and employed in pollution control applications (selective catalytic oxidation/reduction) and during some industrial processes.

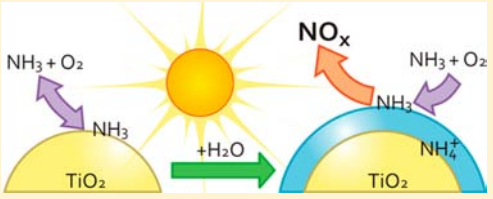

INTRODUCTION

Ammonia released to the atmosphere by agriculture,[1] natural terrestrial and marine sources,[2] and by three-way catalysts on automobiles[3] is an ubiquitous component of air, with concentrations ranging from <50 ppt in remote areas to 0.2−60 ppb in urban and agricultural areas.[4,5] The reaction of NH_3 with OH radical in the gas phase is slow,[6] rendering this an ineffective removal pathway. Deposition of NH_3 onto surfaces or reaction with H_2SO_4 and HNO_3 is commonly regarded as the primary atmospheric fate of ammonia.[7,8] However, we show here that atmospherically relevant levels of NH_3 are photochemically oxidized to NO_x ($NO_x \equiv NO + NO_2$) on TiO_2, which is included in paints, glass, and ceramics formulations for its favorable physical-chemical and photocatalytic properties.[9−11] Titanium dioxide is also used in remediation processes[12] and is being considered as a geoengineering material to be injected into the upper atmosphere in efforts to mitigate the effects of climate change.[13] In rural areas there has been interest in using TiO_2-based photocatalytic devices to mitigate air emissions of odorous volatile organic compounds, hydrogen sulfide, and NH_3 from concentrated animal feed operations.[14] Likewise, there is interest in devising "self-cleaning" coatings for reducing both indoor and outdoor air pollution.[11,15] We show that uptake of atmospheric NH_3 onto surfaces containing TiO_2 is not a permanent removal process, as previously thought, but rather a photochemical route for generating reactive oxides of nitrogen that play a role in air pollution and are associated with significant health effects.[16,17]

Nitrogen oxides, such as NO and NO_2, are byproducts of combustion and precursors of ozone, nitric acid, and secondary organic aerosol.[5] Studies have shown that heterogeneous photochemistry on metal oxides and soil surfaces can regenerate gas-phase NO_x in a process termed "renoxification".[18−23] These previous studies focused on photochemical reduction of nitrate to NO_x and the conversion of NO_2 to NO and HONO using photocatalysts, such as TiO_2 and organic chromophores present in humic acid and soot. Due to the abundance of ammonia in the lower atmosphere, a mechanism of NH_3 oxidation could be a potentially important source of NO_x to consider, especially in the vicinity of buildings or urban infrastructure with TiO_2-coated surfaces.

Titanium dioxide band gap excitation (3.2 eV) generates excited-state conduction-band electrons (e_{cb}^-) and valence-

Received: February 20, 2013
Published: May 30, 2013

   dx.doi.org/10.1021/ja401846x | J. Am. Chem. Soc. 2013, 135, 8606−8615

band holes (h_{vb}^+) that undergo electron-transfer reactions with adsorbed electron donors or acceptors. In the presence of atmospheric O_2 and adsorbed water, oxidants, such as superoxide and hydroxyl radicals, are also generated:[11,12]

$$TiO_2 + h\nu(\lambda < 400\ nm) \rightarrow e_{cb}^- + h_{vb}^+ \quad (1)$$

$$e_{cb}^- + O_2 \rightarrow O_2^- \quad (2)$$

$$h_{vb}^+ + H_2O \rightarrow OH + H^+ \quad (3)$$

Driven by more stringent emissions standards, TiO_2 photocatalysts have been studied for use in removing NH_3 from industrial exhaust streams via photolytic selective catalytic oxidation (photo-SCO).[24−29] Flow reactors containing a bed of TiO_2 powder over which gaseous NH_3 is reacted have been used to monitor photochemical product formation. These studies show that photochemistry initiates the catalytic oxidation of ammonia to molecular nitrogen and N_2O.[27] Experiments carried out on these systems use high concentrations of NH_3, often in the parts-per-thousand (ppth) range, making it difficult to extrapolate the observed chemistry to atmospheric conditions. In addition, this previous work on photo-SCO has focused on the efficiency of N_2 or N_2O production instead of on products, such as NO_x. In a related technology, selective catalytic reduction (SCR) has been employed as a flue gas or diesel emissions treatment and shares with photo-SCO common intermediate reaction steps that reduce NO_x to N_2 via reactions involving NH_3.[30,31] There has been much interest in developing TiO_2 photocatalysts that could be used for SCR at near ambient temperatures.[26,32] It is important to understand under which conditions these emerging technologies are effective and whether there are any drawbacks associated with their use (e.g., the formation of harmful byproducts).

Here we use a chemiluminescence NO_x analyzer coupled to a coated-wall flow tube and diffuse reflection infrared Fourier transform spectroscopy (DRIFTS) to study the photochemistry of NH_3 initiated on TiO_2 surfaces. To our knowledge this is the first study of NH_3 oxidation on TiO_2 surfaces under conditions of relative humidity (RH, 0−90%) and NH_3 concentrations (0−332 ppb) that are typical of the lower atmosphere. Combined with theoretical calculations that provide a molecular-level understanding of the catalytic role of water on the $NH_2 + O_2$ reaction and support the experiments, this work advances our understanding of the mechanism of ammonia oxidation on surfaces and provides important insights into the role of water in this chemistry. This work also improves our understanding of the mechanism of photo-SCO (and SCR) processes under atmospherically relevant conditions and is important for assessing the importance of a previously unrecognized source of nitrogen oxides from TiO_2-containing surface coatings.

METHODS

Preparation and Characterization of TiO_2 Surfaces. Anatase powder (99.8%) and Evonik (Degussa) Aeroxide P25 were purchased from Sigma-Aldrich, while rutile was obtained from Inframat Advanced Materials. All experiments were carried out using anatase powder except for comparative trials that used P25 and rutile photocatalysts. Powder X-ray diffraction (XRD, PANalytical Empyrean) data were used to confirm the crystalline phase of the photocatalyst powders. The surface area of the anatase powder is 8.6 $m^2\ g^{-1}$, as determined by Brunauer−Emmett−Teller (BET) analysis of N_2 adsorption isotherms that were obtained with a Micrometrics ASAP 2020 physisorption analyzer; Barrett−Joyner−Halenda analysis was used to determine the pore size distribution of the sample. The anatase sample has an average particle size of 0.6 μm, and 90% of the particles have a diameter of <1 μm, according to manufacturer specifications. Samples used for flow tube experiments were heated to 475 °C overnight in air to remove organic contaminants. Analyses of the sample before and after heating with XRD show that this procedure does not change the crystalline phase of the sample. For flow tube experiments, the inner surface of a 1.54 cm i.d. glass tube was coated with a slurry of TiO_2 in water using a radial brush. The coated tubes were then dried by heating in an oven (120 °C) overnight and stored in a desiccator prior to use. This method consistently yielded an even coating weighing 44 ± 1 mg (dry weight). The total surface area of anatase coatings irradiated with UV−vis radiation during the experiments is 0.35 ± 0.1 m^2 (the indicated error represents 95% confidence intervals of the mean of 45 samples). A newly coated surface was used for each experiment.

Coated-Wall Flow Tube Experiments. Photochemical experiments were carried out in a jacketed (296 ± 0.02 K) Pyrex horizontal flow tube (100 × 2 cm i.d.) that is operated in a similar fashion to other well-documented systems.[20,33−35] Ammonia from a permeation device (420 ng min^{-1}, VICI Metronics) is mixed with the RH-stabilized diluent air at 1 atm and exited the flow tube through a conical port at the opposite end. The RH of the diluent air is adjusted by mixing dry and humid air (from a water bubbler) in a 4 L mixing bulb equipped with a RH and temperature probe (Vaisala, HMT130). The total flow of gas exiting the flow tube is 2570 $cm^3\ min^{-1}$. The smaller glass tube containing the TiO_2 coating is positioned inside the flow tube. All glass surfaces with the exception of the TiO_2-coated tube are coated with a hydrophobic and inert perflourinated polymer (Fluoropel PFC 801A, Cytonix Corp.) and Teflon tubing, and fittings are used throughout to minimize gas−wall interactions. The Reynolds number of the reactor under these conditions is 181, indicating that experiments were conducted under laminar flow conditions. The NO and NO_2 concentrations are measured by subsampling (470 $cm^3\ min^{-1}$) the reaction effluent with a chemiluminescence NO_x analyzer (Teledyne Model 200E) that has a detection limit of 0.2 ppb for both NO and NO_2. The accuracy of the NO_x analyzer was verified via comparisons to concentrations measured by a long-path FTIR (Bruker Optics, Vertex 70 FTIR, 22.4 m path length); agreement between FTIR and the NO_x analyzer is within 3% for both NO and NO_2.

Two Xe−Hg arc lamps (200 W, Spectra Physics) mounted on the outside of the flow tube are used to uniformly irradiate the 8 cm length of TiO_2 coating. The lamps are equipped with a dichroic mirror placed between the lamp and a 290 nm cutoff filter to minimize heating of the sample by infrared radiation from the lamp. The spectrum of the photolysis light source consists of wavelengths >290 nm, with several intense Hg lines between 350 and 450 nm. Photolysis of NO_2 was used as an actinometer to determine the lamp intensity and to correct for secondary photolysis of NO_2 during the NH_3 oxidation experiments. A continuous stream of NO_2 (19 ppb in 1 atm of air) was passed through the flow tube under conditions that were identical to the photochemical experiments described above. The concentration of NO and NO_2 was determined before and after the lamps were turned on. The first-order rate constant, $J(NO_2)$, is calculated from[36]

$$J(NO_2) = \frac{1}{t}\frac{\Delta[NO]}{[NO_2]_0} \quad (4)$$

where $\Delta[NO]$ is the amount of NO formed during the experiment, $[NO_2]_0$ is the concentration of NO_2 before photolysis, and t is the residence time of gas in the irradiated section of the flow tube. The value of $J(NO_2)$ was determined to be 0.065 s^{-1}. Accounting for the spectrum of the lamps and the known absorption cross sections and quantum yields for NO_2 photolysis,[5] we calculated the light intensity of the lamps (300−420 nm) to be 9.0×10^{16} photons $s^{-1}\ cm^{-2}$. At this intensity, NO_2 loss was 2.5%. While the observed NO/NO_2 ratio is affected by secondary photolysis of NO_2, the total NO_x values and the calculated uptake coefficients are insensitive since photolysis of NO_2 will yield NO quantitatively.

dx.doi.org/10.1021/ja401846x | J. Am. Chem. Soc. 2013, 135, 8606−8615

Derivation of Reactive Uptake Coefficients. The reactive uptake coefficient (γ) is the fraction of collisions of NH_3 with the TiO_2 surface that remove NH_3 from the gas phase due to chemical reactions yielding NO_x.[37] The uptake coefficient can be expressed as

$$\gamma = \frac{2rk_{obs}}{\omega} \quad (5)$$

where r is the radius of the TiO_2-coated tube, and the average molecular speed of NH_3 is given by $\omega = (8RT/\pi M)^{1/2}$, where R, T, and M are the gas constant, absolute temperature, and the molecular weight of NH_3, respectively. Using a previously reported approach, the first-order rate coefficient k_{obs} for the reaction of $NH_3 \rightarrow NO_x$, is calculated from[38]

$$k_{obs} = -\frac{1}{t}\ln\left(\frac{[NH_3]_0 - [NO_x]_{ss}}{[NH_3]_0}\right) \quad (6)$$

where t is the residence time of NH_3 in contact with the TiO_2 surface in the flow reactor and $[NO_x]_{ss}$ is the steady-state concentration of NO_x reached during a photolysis experiment. The γ-values reported here have been corrected for axial and radial diffusion using the Cooney–Kim–Davis method,[39,40] using a diffusion coefficient of 0.28 $cm^2\ s^{-1}$ for NH_3 in 1 atm of air at 296 K.[41] Note that all uptake coefficients reported here are based on the geometric surface area of the TiO_2 coating. The TiO_2 coating is porous and diffusion to and reaction within interstitial spaces likely contributes to NH_3 uptake.[9,42] To take into account the total substrate surface area accessible to NH_3, a mass-independent uptake coefficient can be derived from the BET-derived surface area by multiplying the γ-values reported here by 1.8×10^{-2}.

DRIFTS. The adsorption of gaseous ammonia onto TiO_2 particles was studied with DRIFTS. A powder sample of TiO_2 (0.15 g) was packed into the sample holder (geometric surface area of 0.32 cm^2) of a stainless steel diffuse reflection reaction chamber (Harrick Scientific, HVC-DRP-4) that is mounted in the sample compartment of the Fourier transform infrared spectrometer (Bruker Optics, Vertex 70 FTIR). The chamber cover contains two IR-transmissive KBr windows and one quartz window. A set of mirrors located in the FTIR sample compartment transfers light from the IR source to the sample and efficiently collects diffusely reflected IR light (minus the specular component) for detection by the spectrometer's liquid nitrogen-cooled Hg–Cd–Te detector. Due to the short path length (2 cm) of the IR beam through the headspace of the chamber, ppb levels of species present in the gas-phase above the substrate are undetectable. Each spectrum is derived by averaging 512 spectra collected at a resolution of 8 cm^{-1}.

Air containing NH_3 in air was flowed through the TiO_2 substrate at a rate of 85 $cm^3\ min^{-1}$ to study the adsorption of NH_3 onto the surface. Experiments were conducted at 0, 4, and 27% RH at 298 K and 1 atm total pressure, while the NH_3 concentration was held constant at 740 ppb. Before the dry experiment the TiO_2 powder was heated in the DRIFTS sample holder at 475 °C for 1 h, cooled to room temperature, and then left overnight under a constant flow of dry air. The next day, ammonia was added to the flow while spectra were collected. Before introducing RH stabilized air the TiO_2 powder was packed into the sample holder and heated in situ at 475 °C for 5 h, cooled to room temperature, and then exposed to humid air at a flow rate of 85 $cm^3\ min^{-1}$. After 1 h, the sample was exposed to ammonia while spectra were collected.

Computational Details. To investigate the influence of water on NH_2 oxidation, small water clusters were used as a surrogate to model the interactions of intermediates with the thin water films present on experimental surfaces. We have successfully used this approach in the past to investigate the role of water in catalyzing surface reactions.[43] Reactants, intermediates, and products of the $NH_2 + O_2 + (H_2O)_n$ (n = 0–5) reaction were optimized using second-order Møller–Plesset perturbation theory (MP2)[44] with an unrestricted Hartree–Fock (UHF) reference and the aug-cc-pVTZ basis set.[45,46] The doublet NH_2 and triplet O_2 reactants yield doublet intermediates. The expectation values of the S^2 operator fell between 0.75 and 0.78 for the intermediates indicating some, but not severe, spin contamination.[47] Harmonic frequencies were calculated to obtain the zero-point energy (ZPE) correction, and natural population analyses were carried out to determine the partial charges.[48] For the unsolvated reaction and for the reaction of NH_2 and O_2 with $(H_2O)_2$, the energies were also calculated at the coupled cluster singles and doubles level with a perturbative triples correction (CCSD(T))[49] to estimate the effect of additional electronic correlation. In all calculations the core electrons were excluded from correlation, and auxiliary basis sets[50] were used in conjunction with the resolution-of-identity approximation to reduce computational cost. Optimizations, harmonic frequency calculations, and single-point energy determinations were performed with the TURBOMOLE program package.[51]

RESULTS AND DISCUSSION

Photochemical Uptake of NH_3 on TiO_2 Surfaces. We initially studied the photocatalytic conversion of NH_3 to NO_x on TiO_2 coating the wall of the flow reactor operated at 40% RH. Figure 1a shows that a TiO_2 film exposed to a continuous flow of 9 ppb NH_3 in humidified air is unreactive in the dark but generates NO_x when irradiated with UV–vis light. During irradiation, the NO_x concentration stabilizes to a steady-state concentration of ~3 ppb between 40–50 min. This amounts to a 33% yield of NO_x, relative to the initial gas-phase concentration of NH_3 entering the flow tube, $[NH_3]_0$. The NO_x signal returns to baseline when the lamps are turned off. A similar experiment was carried out by exposing TiO_2 to a continuous flow of NH_3 in nitrogen (Figure 1b). In this case, irradiation of the surface with UV–vis light generated a negligible amount of NO_x. This demonstrates that O_2 is a reactant in the mechanism that forms NO_x. Control experiments were carried out before each experiment to determine the amount of background NO_x emitted from the TiO_2 substrate in the absence of added NH_3. Nitric oxide was always below the detection limit of the instrument, while the amount of background NO_2 emitted was consistently below 1 ppb. The control experiments were used to correct the NO_2 concentrations measured when NH_3 was photooxidized.

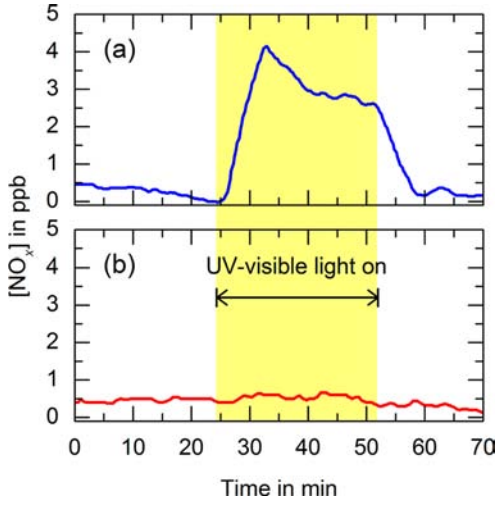

Figure 1. Increase in NO_x concentration as TiO_2 is irradiated (λ > 290 nm) in the presence of 9 ppb of NH_3 at 40% RH in 1 atm of (a) air or (b) nitrogen at 296 K.

The most common TiO_2-based photocatalysts used in commercial applications are anatase or mixtures of anatase and rutile phases [e.g., Evonik (Degussa) Aeroxide P25, a 70:30 mixture of anatase and rutile].[52–55] We compared the

dx.doi.org/10.1021/ja401846x | J. Am. Chem. Soc. 2013, 135, 8606–8615

photoreactivity of the anatase photocatalyst described above to rutile and P25 under identical experimental conditions. A stream of air containing 22 ppb of NH_3 was flowed over the photocatalyst (at 48% RH and 296 K), and the amount of NO_x formed was monitored. Relative to anatase, the P25 photocatalyst produced twice as much NO_x, while the reactivity of rutile was <10% that of anatase. The differences in activity are ascribed to well-known differences in band gap energies, adsorptive capacities, and electron−hole recombination efficiencies of the various catalysts.[56] For example, the P25 sample has the highest surface area (53 m^2 g^{-1}) and the lowest electron−hole recombination rate, while rutile has the lower surface area (8 m^2 g^{-1}) and is expected to have the highest electron−hole recombination rate. Experiments described below were carried out on the pure anatase photocatalyst to limit our interpretation to reactions occurring on a homogeneous crystalline phase.

The conversion of NH_3 to NO_x on irradiated TiO_2 surfaces was investigated at initial NH_3 concentrations ranging between 0−332 ppb in air. The humidity of the carrier gas was maintained at 48 ± 2% to reflect typical atmospheric conditions. Figure 2a shows that the amount of NO_x formed increases as $[NH_3]_0$ increases. At NH_3 concentrations above 150 ppb the steady-state NO_x concentration remains constant at ∼25 ppb. To examine the efficiency of the reaction, we plot the reactive uptake coefficient of NH_3 on irradiated TiO_2 surfaces as a function of NH_3 concentration in Figure 2b. The inverse dependence of the reactive uptake coefficients on the NH_3 concentration is consistent with a Langmuir−Hinshelwood mechanism, whereby NH_3 reversibly adsorbs to irradiated TiO_2 surface sites before undergoing a reaction that generates NO_x. In this mechanism, the decrease in γ at higher $[NH_3]_0$ is explained if the available reactive sites on the TiO_2 surface become saturated with adsorbed NH_3 molecules, preventing further collisions with reactive sites. Similar uptake behavior is observed for a number of atmospherically relevant heterogeneous reactions, including the reaction of NO_2 on irradiated surfaces comprised of TiO_2 or mineral dust.[18,57] As discussed below, it is also possible that SCR of NO_x to N_2 at higher $[NH_3]_0$ also contributes to the decrease in the uptake coefficient.

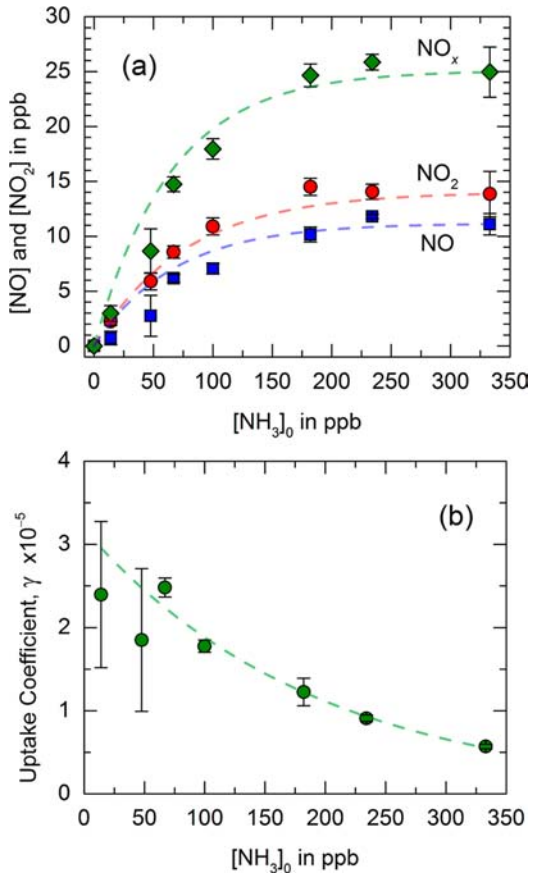

Figure 2. (a) Steady-state concentration of NO_x, NO, and NO_2 achieved during UV−vis irradiation of TiO_2 surfaces depends on the initial concentration of NH_3. (b) Dependence of the uptake coefficient (γ) of NH_3 on TiO_2 coatings as a function of initial NH_3 concentration. Data were collected at a RH of 48% in 1 atm of air at 296 K. Error bars are 95% confidence intervals of replicate experiments. Fitted lines are guides for the eye.

The sensitivity of NH_3 photooxidation toward adsorbed water was investigated by varying the RH of the air between 0 and 90% while maintaining the $[NH_3]_0$ at 67 ppb. Figure 3a shows that the amount of NO_x formed increases as the RH is raised from 0 to 50%. Between 40 and 50% RH, the concentration of NO_x in the flow tube reaches a maximum of 15 ppb, but it decreases if the humidity is increased to above 50%. The uptake coefficients shown in Figure 3b reflect this and show that conversion of NH_3 to NO_x is most efficient at

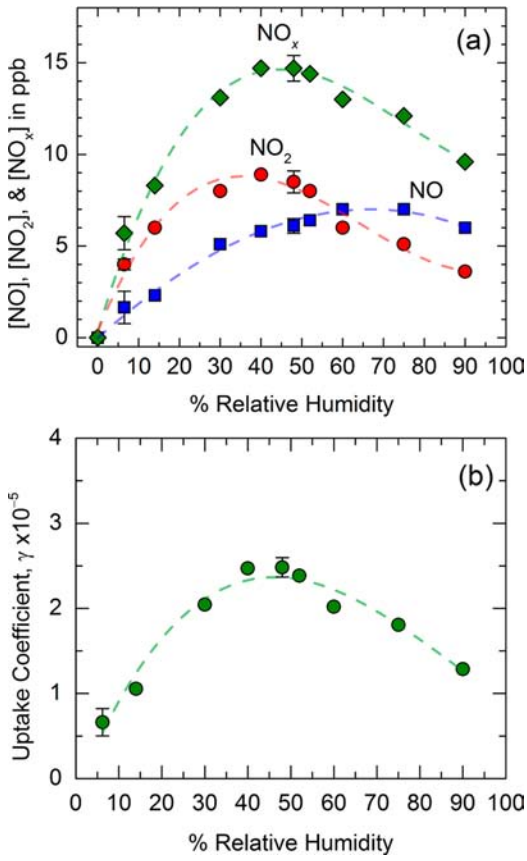

Figure 3. Plots of (a) the steady-state concentration of NO, NO_2, and NO_x formed and (b) the reactive uptake coefficient as a function of percent RH. Data were collected using an initial NH_3 concentration of 67 ppb in 1 atm of air at 296 K. Error bars are 95% confidence intervals of replicate experiments. Fitted lines are guides for the eye.

dx.doi.org/10.1021/ja401846x | J. Am. Chem. Soc. 2013, 135, 8606−8615

between 40−50% RH. This suggests that the mechanisms leading to NO_x is water catalyzed. However, at high RH it appears that another mechanism becomes important, whereby additional surface-adsorbed water hinders the formation of NO_x. The relative yields of NO and NO_2 are also highly dependent on the humidity of the air. As shown in Figure 3a, at between 0 and 50% RH the amount of NO_2 formed is higher than that of NO. However, if the RH is >60%, NO is the dominant species detected.

Ammonia Speciation on TiO_2. Infrared spectroscopy was used to understand the speciation of NH_3 on the TiO_2 surface under the conditions of our flow tube experiments. A diffuse reflection infrared spectrum of TiO_2 powder in equilibrium with a flow of 740 ppb of NH_3 in dry air at 1 atm is shown in Figure 4a. The peaks at 3408, 3368, and 3265 cm^{-1} are N−H

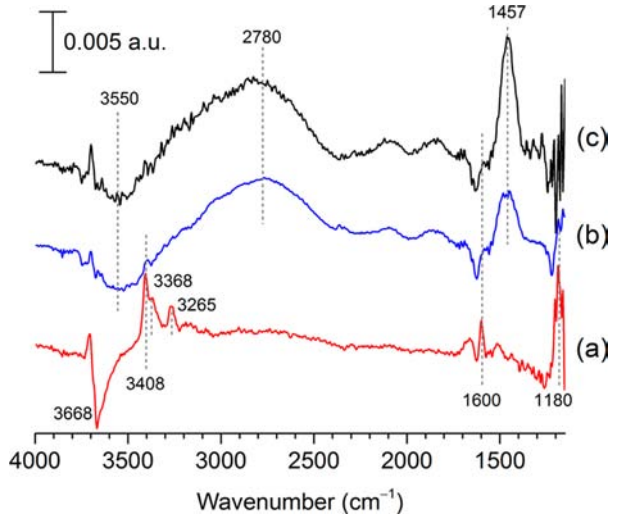

Figure 4. Diffuse reflection IR spectra of TiO_2 exposed to 740 ppb of NH_3 in air (1 atm) at (a) 0%, (b) 4%, and (c) 27% RH. The *y*-axis is $\log_{10}(S_0/S)$, where S_0 is the background spectrum of pure TiO_2 powder and S is the spectrum of TiO_2 after 120 min exposure to the NH_3/air mixture. All experiments were done at 298 K.

stretching vibrations, while the bands at 1600 and 1180 cm^{-1} are due to the asymmetric and symmetric deformation modes of NH_3 coordinated to TiO_2.[58] Adsorption of NH_3 to the surface coincides with the appearance of a negative peak centered at ∼3670 cm^{-1}, corresponding to the loss of free surface O−H groups upon NH_3 adsorption. When the experiment is repeated at 4 and 27% RH, the bands due to adsorbed NH_3 are undetectable (Figure 4b,c). Instead, a broad peak centered at 2780 cm^{-1} and an intense peak at 1457 cm^{-1} appear in the spectra.[58] These are due to the N−H stretching and deformation vibrations of NH_4^+, respectively.[59] Ammonia is converted to NH_4^+ on the TiO_2 surface according to[60,61]

$$NH_3 + H_2O \rightleftharpoons NH_4^+ + OH^- \quad (7)$$

The FTIR results suggest this reaction occurs readily on TiO_2 even at low RH. A broad negative peak appears at 3600 cm^{-1} in Figure 4b,c due to changes on the surface as Ti−OH groups, which are hydrogen bonded to water, become involved with interactions with NH_4^+ as ammonia is added. The OH^- formed in eq 7 is not discernible at the expected position of ∼3600 cm^{-1};[62] the peak would be significantly broadened by interactions with solvating water, and its position overlaps with the negative peak occurring at the same position in the spectra.[63,64]

Mechanism of NH_3 Oxidation. The initial step of ammonia oxidation stems from the collision of NH_3 with a valence band hole on the TiO_2 surface:

$$NH_3 + h_{vb}^+ \rightarrow NH_2 + H^+ \quad (8)$$

This hole-transfer reaction would result in formation of the amino radical, NH_2, which has been observed in previous studies of NH_3 oxidation on TiO_2 by electron paramagnetic resonance spectroscopy.[28] It is also possible that OH radicals generated on the TiO_2 surface from eq 3 react with NH_3 by abstracting a hydrogen atom to form the amino radical:

$$NH_3 + OH \rightarrow NH_2 + H_2O \quad (9)$$

The second-order rate coefficient for this reaction in the gas phase is 1.6×10^{-13} cm^3 $molecule^{-1}$ s^{-1}.[6] At high OH levels, recombination to H_2O_2 is expected to moderate the concentration of OH available to react with NH_3.[12] Although a significant amount of adsorbed NH_4^+ is observed in the FTIR spectra when TiO_2 is exposed to NH_3 in the presence of water, the reactive precursor responsible for the NO_x in the flow tube experiments is most likely NH_3. Previous work suggests that NH_4^+ is unreactive toward OH radical in aqueous solutions.[65,66] Ammonium is not easily oxidized photochemically by TiO_2, as its oxidation potential lies above the conduction band edge of TiO_2. For example, it is known that electrochemical oxidation of NH_4^+ is only possible in solutions with a pH above 9, where NH_3 is the dominant species.[67,68] Thus, formation of NH_4^+ on thin water films at high RH is a terminal sink for ammonia that competes with eqs 8 and 9.

Although several routes to NO_x may be proposed, a mechanism that describes the fate of NH_2 and considers the role of O_2 and H_2O in the reaction is as follows:[69]

$$NH_2 + O_2 + H_2O \rightarrow (NH_2OO)\cdot(H_2O) \quad (10)$$

$$(NH_2OO)\cdot(H_2O) \rightarrow (NHOOH)\cdot(H_2O) \quad (11)$$

$$(NHOOH)\cdot(H_2O) \rightarrow NO + 2H_2O \quad (12)$$

$$\text{net reaction:} \quad NH_2 + O_2 \rightarrow NO + H_2O \quad (13)$$

Consistent with the observation that the reaction depends on O_2, we propose that the next step is the addition of O_2 to NH_2 to form an aminoperoxy radical (NH_2OO).[69] In the gas phase, NH_2 reacts slowly with O_2, with a second-order rate constant of $\leq 6 \times 10^{-21}$ cm^3 $molecule^{-1}$ s^{-1}.[5] However, the reaction is rapid in the aqueous phase, with a second-order rate constant of $\sim 10^9$ L mol^{-1} s^{-1} (i.e., $\sim 2 \times 10^{-12}$ cm^3 $molecule^{-1}$ s^{-1}).[69] Nitric oxide is formed when the resulting NH_2OO species undergoes water-catalyzed isomerization followed by decomposition.[69] As indicated by eqs 10−12, water is not only required in the mechanism leading to NO but also generated as a product in the mechanism. Thus, surface-adsorbed water acts as a catalyst in the mechanism. Once formed, NO is oxidized to NO_2 on the TiO_2 surface via its reaction with trapped holes (i.e., oxygen anion radicals covalently bonded to titanium) on the irradiated TiO_2 surface:[23,70,71]

$$Ti^{4+}{-}O^- + NO \rightarrow Ti^{4+}{-}ONO^- \rightarrow Ti^{3+} + NO_2 \quad (14)$$

Surface morphology of the photocatalyst likely plays an important role in the observed reactivity. Nitrogen adsorption and desorption isotherms were measured to determine the

dx.doi.org/10.1021/ja401846x | J. Am. Chem. Soc. 2013, 135, 8606−8615

surface area and pore size distribution of the anatase substrate used in the NH_3 photooxidation measurements. The adsorption branch of the isotherm is type II according to the IUPAC classification, which is typical of macroporous adsorbents.[72] A weak hysteresis observed at $p/p_0 > 0.8$ suggests capillary condensation of N_2 in the sample occurs.[72] The pore size distribution plotted in Figure 5 shows the sample consists

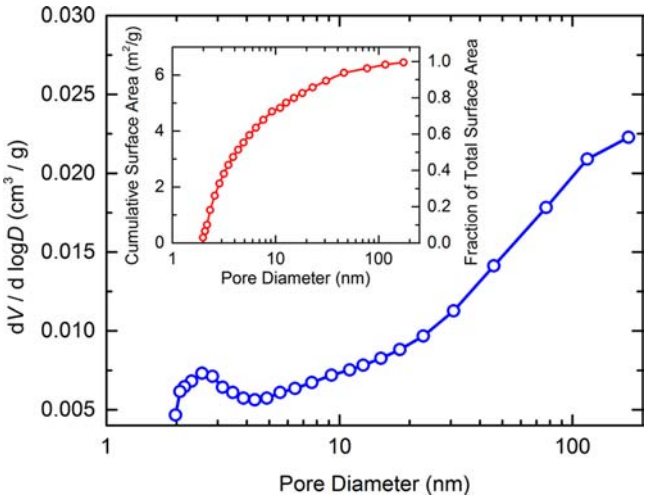

Figure 5. Pore size distribution derived from the nitrogen adsorption isotherm of anatase powder. A plot of the cumulative surface area for pores with diameters between 1.9 and 173 nm is shown in the inset.

of macropores with diameters from 50 to >100 nm. Mesopores having diameters between 2 and 50 nm are also present, with a peak at 2.5 nm. A total pore volume of 0.024 cm^3/g was determined from the absorption isotherm at $p/p_0 = 0.99$. The cumulative surface area plotted in Figure 5 (inset) shows that ~80% of the total surface area available for reaction is present in mesopores that are <15 nm in diameter.

Interaction of H_2O with TiO_2 in the mesopores likely leads to capillary condensation of water at vapor pressures below what is expected for equilibrium vapor pressure of H_2O with a planar surface.[73,74] The RH at which mesopores fill up with water is estimated from the Kelvin equation:

$$\frac{p}{p_{sat}} = \exp\left[-\frac{\sigma V_m}{RT}\left(\frac{1}{r_1} + \frac{1}{r_2}\right)\right] \quad (15)$$

where p/p_{sat} is RH, σ is the surface tension of water, V_m is the molar volume of water, and r_1 and r_2 are the two principle radii of curvature of the meniscus. According to eq 15 a pore with a 2.5 nm diameter will fill up at either 43 or 66% RH, depending on whether a hemispherical ($r_1 = r_2 = 1.25$ nm) or cylindrical ($r_1 = 1.25$ nm; $r_2 = \infty$) pore geometry is assumed. Interestingly, this encompasses the RH range in which $NH_3 \rightarrow NO_x$ conversion appears to be most efficient in Figure 3. It is therefore possible that mesopores, which contribute significantly to the total surface area, play an important role in providing sites for both water adsorption and surface reactions. Once filled with water, diffusion of precursors into the mesopores is limited, and photooxidation occurs mainly in macropores and the external surface, which provide lower surface area for reactions to occur on; not only would this result in fewer sites for NH_3 to react on at high RH but also would limit $NO \rightarrow NO_2$ conversion and explain why NO_2 transitions from being the major product at RH < 60% to being the minor product at RH > 60%. The presence of multilayers of water in mesopores would also explain the FTIR results showing that NH_3 is converted to NH_4^+ even at low RH. It is therefore likely that the reduced NO_x yield observed in Figure 3a at high RH is due to filling of mesopores with water, formation of unreactive NH_4^+, and reduced oxidant levels due OH radical recombination.

Role of Water in Catalyzing NH_3 Oxidation. A theoretical investigation was carried out to further elucidate the role of water in catalyzing the proposed reaction of NH_2 with O_2. Beginning with structures for the NH_2OO and NHOOH intermediates previously studied by Sumathi and Peyerimhoff,[75] $NH_2OO\cdot(H_2O)_n$ and $NHOOH\cdot(H_2O)_n$ (n = 1−5) clusters were constructed and optimized at the MP2/aug-cc-pVTZ level. Preliminary calculations indicated that $(H_2O)_2$, but not a single H_2O, can form a hydrogen-bonding network that solvates one side of the NH_2OO intermediate and that $(H_2O)_5$ forms a hydrogen-bonding network solvating both sides of the NH_2OO intermediate. For $n = 6$, clusters similar to those found for $n = 5$ were obtained, but with minor structural or energetic differences. These results will not be included here.

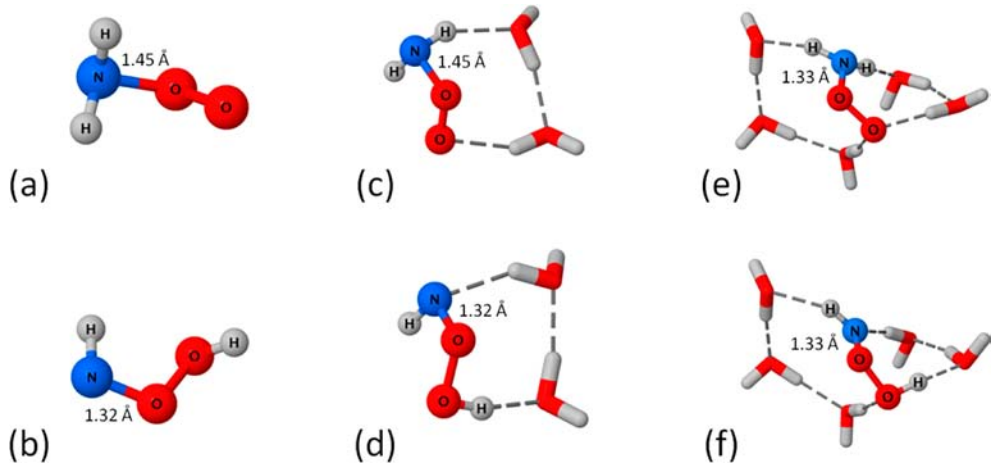

Figure 6. Intermediate structures determined at the MP2/aug-cc-pVTZ level of theory for (a) NH_2OO, (b) NHOOH, (c) $NH_2OO\cdot(H_2O)_2$, (d) $NHOOH\cdot(H_2O)_2$, (e) $NH_2OO\cdot(H_2O)_5$, and (f) $NHOOH\cdot(H_2O)_5$ with the N−O bond distance indicated.

dx.doi.org/10.1021/ja401846x | J. Am. Chem. Soc. 2013, 135, 8606−8615

Minimum energy structures for the bare intermediates and the $NH_2OO\cdot(H_2O)_n$ and $NHOOH\cdot(H_2O)_n$ (n = 2, 5) clusters are presented in Figure 6. Upon solvation of NH_2OO, the N−O bond distance remains largely unchanged for $(H_2O)_2$ but decreases significantly from 1.45 to 1.33 Å for $(H_2O)_5$, approaching the value for the HNOOH intermediate (r_{NO} = 1.32−1.33 Å). This decrease in the N−O bond distance is associated with an increase in the partial charge on the NH_2 and O_2 fragments of NH_2OO in the n = 5 cluster [$\delta(NH_2)$ = +0.5; $\delta(O_2)$ = −0.5] compared to that of unsolvated NH_2OO and in the n = 2 cluster [$\delta(NH_2)$ = +0.2; $\delta(O_2)$ = −0.2].

Solvation in both the $NH_2OO\cdot(H_2O)_2$ and $NH_2OO\cdot(H_2O)_5$ clusters is accompanied by a rotation about the NO bond to form a nearly planar OONH structure, similar to that of the HNOOH intermediate. The water network surrounding the NH_2OO intermediate supports or induces conformational changes to reduce the structural differences between NH_2OO and NHOOH intermediates. All that remains for the conversion of NH_2OO to NHOOH is transfer of a proton from the NH_2 group to the terminal oxygen of NH_2OO. The hydrogen-bonded network of the surrounding waters is conveniently at hand and may provide a low-energy path for this process through proton transfer along a water wire. For conversion of NHOOH to NO + H_2O we must look to the $NHOOH\cdot(H_2O)_5$ cluster which has a hydrogen-bonded network in place to transfer the remaining NH proton to the terminal O of NHOOH. Again, the solvating waters may allow for proton transfer along a water wire, thus avoiding the high barriers for conversion between NO + H_2O and NHOOH that makes this reaction unlikely in the gas phase.[75]

The above observations concerning structural features suggest that the primary role of water in the NH_2 + O_2 reaction to NO + H_2O is to lower reaction barriers. By looking at the energies of the intermediate clusters relative to the reactants, it is also clear that when solvated by two or five water molecules the NH_2OO and NHOOH intermediates form stable clusters. The relative energies of the $NH_2OO\cdot(H_2O)_n$ and $NHOOH\cdot(H_2O)_n$ (n = 0, 2, 5) intermediates at the MP2 and CCSD(T) levels are collected in Table 1. At the MP2/aug-cc-pVTZ level the unsolvated intermediates are nearly isoenergetic to the reactants. The higher-level CCSD(T) calculations indicate that these intermediates are very weakly bound relative to the reactants and that this additional correlation makes a more significant contribution to the relative stability of NH_2OO (−4.6 kcal/mol) versus NHOOH (−2.2 kcal/mol). The CCSD(T) calculations also indicate that the NH_2OO-to-NHOOH isomerization in the bare system is slightly endothermic, as was noted previously.[75] Formation of the solvated intermediates $NH_2OO\cdot(H_2O)_2$ and $NHOOH\cdot(H_2O)_2$ from O_2 + NH_2 + $(H_2O)_2$ is energetically favorable at the MP2 level, and the additional correlation contributions to the NH_2OO cluster (−4.0 kcal/mol) and the NHOOH cluster (−2.0 kcal/mol) are very similar to the contributions for the bare species. Upon solvation the second intermediate, NHOOH, becomes more stable than the first intermediate, NH_2OO, yielding an exothermic isomerization.

Table 1. Energies of $NH_2OO\cdot(H_2O)_n$ and $NHOOH\cdot(H_2O)_n$ Intermediates Relative to NH_2 + O_2 + $(H_2O)_n$ [n = 0, 2, 5]

species	MP2/aTZ[a] (kcal/mol)	MP2/aTZ//CCSD(T)/aTZ[b] (kcal/mol)
NH_2OO	0.2	−4.4
NHOOH	−1.3	−3.5
$NH_2OO\cdot(H_2O)_2$	−7.7	−11.7
$NHOOH\cdot(H_2O)_2$	−13.6	−15.6
$NH_2OO\cdot(H_2O)_5$	−4.7	–
$NHOOH\cdot(H_2O)_5$	−8.8	–

[a]Structures, zero-point corrections, and energies determined at the MP2/aug-cc-pVTZ level. [b]Structures and zero-point corrections determined at the MP2/aug-cc-pVTZ level; energies determined at the CCSD(T)/aug-cc-pVTZ level.

The smaller magnitude of the relative energies of the $NH_2OO\cdot(H_2O)_n$ and $NHOOH\cdot(H_2O)_n$ clusters for n = 5 compared to those for n = 2 can be attributed to the energy required to insert a solute into the hydrogen-bonding structure of water. In the n = 2 clusters, the water dimer is only slightly distorted from preferred geometry, whereas for the water pentamer, two hydrogen bonds must be broken to solvate both sides of the NH_2OO and NHOOH intermediates. However, formation of the $NH_2OO\cdot(H_2O)_5$ and $NHOOH\cdot(H_2O)_5$ clusters is still energetically favorable. Formation of the NO + $(H_2O)_{(n+1)}$ products from O_2 + NH_2 + $(H_2O)_n$ (n = 0, 2, 5) is very exothermic with reaction energies from −80 to −90 kcal/mol at the MP2 level and −75 to −85 kcal/mol at the CCSD(T) level. The question is not whether formation of the final products is favorable but whether the intermediates are stable, which this work supports. The primary remaining question to be investigated is the presumed lowering of the barrier heights. Additionally, the role of the TiO_2 surface in the oxidation of NH_2 remains unaddressed in this computational study. In previous work by Laszlo et al., a rapid reaction of NH_2 with O_2 was observed in aqueous solution without TiO_2 present.[69] As the same mechanism for oxidation of the amino radical was assumed in both our work and the previous study, the TiO_2 surface was not included in our computational model. The influence of the TiO_2 surface on the structure of the water[74] surrounding the intermediates and the likelihood of proton transfer, as well as the direct interaction between the intermediates and the TiO_2 surface, would be desirable topics for future study.

Comparison to Previous Work. The results here demonstrate that there are differences in the distribution of products stemming from ammonia photooxidation under atmospheric conditions and previous studies employing high concentrations of NH_3.[24−28] For example, at ∼1 ppth, Yamazoe et al. found that N_2 (∼30% yield) followed by N_2O (∼5% yield) are the main products of NH_3 photooxidation on TiO_2, where the indicated product yields are relative to the initial concentration of NH_3 used;[27,28] nitric oxide was nearly undetectable in their study. At higher concentrations of NH_3 selective catalytic reduction of NO_x proceeds according to the following net reactions:[30]

$$4NH_3 + 4NO + O_2 \rightarrow 4N_2 + 6H_2O \quad (16)$$

$$4NH_3 + 2NO_2 + O_2 \rightarrow 3N_2 + 6H_2O \quad (17)$$

Intermediate steps to these reactions may also include dimerization of NH_2 radicals to form hydrazine (N_2H_4) or the reaction of NH_2 with NO to form NH_2NO, which at high concentrations would render the NH_2 + O_2 channel (eq 10) insignificant. Surface-adsorbed N_2H_4 and NH_2NO may in turn play a role in the formation of N_2 and N_2O observed in previous studies.[27,30] In our system, eqs 16 and 17 are expected to become more important at higher $[NH_3]_0$ and could

dx.doi.org/10.1021/ja401846x | J. Am. Chem. Soc. 2013, 135, 8606−8615

contribute to the decreased $NH_3 \rightarrow NO_x$ conversion efficiency observed in Figure 2b. It is therefore possible that N_2 could be a significant product in our experiments, although we are unable to confirm this due to analytical limitations that preclude us from measuring N_2. We employed long-path FTIR to determine whether N_2O was formed during experiments where TiO_2 was photolyzed in the presence of 330 and 615 ppb of NH_3 in air at 48% RH and 296 K. In both cases, N_2O was below our detection limit of 9 ppb. This is not surprising since previous studies of SCR processes over V_2O_5 catalysts showed that H_2O suppresses formation of N_2O in favor of N_2.[76,77]

CONCLUSIONS

Our results show that incomplete conversion of NH_3 to N_2 over TiO_2 under atmospherically relevant conditions leads to higher relative yields of NO_x (up to 33%) than what has been observed in concentrated NH_3 streams. Theoretical investigations support a mechanism by which O_2 addition to NH_2 generates an aminoperoxy radical that undergoes water-assisted proton transfer and isomerization to ultimately yield NO and H_2O. Reaction intermediates form stable clusters with $(H_2O)_n$ (n = 2, 5) with a hydrogen-bonded network suited for the necessary proton transfer. Further oxidation of NO on the TiO_2 surface yields NO_2. Above ~50% RH adsorbed water appears to hinder the reaction. Under these conditions, mesopores are likely filled with water due to capillary condensation, which promotes the formation of unreactive NH_4^+ and increases OH recombination kinetics. Reduced access to active sites within mesopores in turn leads to decreased $NH_3 \rightarrow NO$ and $NO \rightarrow NO_2$ conversion efficiency.

Formation of NO_x on TiO_2 surfaces is likely also associated with the formation of adsorbed species, such as NO_3^- and NO_2^-, and potentially nitrous acid (HONO). It is well-known that coadsorption of NO and O_2 on TiO_2 (irradiated with UV–vis light and in the dark) efficiently yields adsorbed nitrate.[23,70] Using FTIR spectroscopy Yamazoe et al. observed nitrate, nitrite, and nitro species formed during the photooxidation of NH_3 over irradiated TiO_2 surfaces when high concentrations of NH_3 (~1 ppth) were employed.[27] It is reasonable to assume that nitrate will be deposited on the surface at the low NH_3 levels used in our study as well. Nitrogen dioxide and NO_3^- are efficiently reduced to nitrous acid (HONO) on TiO_2 surfaces when irradiated with UV–vis light.[18,20,21] Nitrous acid is an important photochemical source of atmospheric OH and NO, which play a role in initiating air pollution chemistry.[5] In addition, it has been suggested that HONO may be an important intermediate during SCR processes that remove NO_2.[29] For example, it is thought that NO_2 hydrolysis in these systems could lead to HONO, which subsequently reacts with NH_3 to form N_2:

$$NH_3 + HONO \rightarrow NH_4NO_2 \rightarrow N_2 + 2H_2O \quad (18)$$

Studies are underway to probe whether secondary reactions stemming from NH_3 photooxidation on TiO_2 under atmospheric conditions generate HONO and what role it may play in subsequent surface reactions of NH_3.

We note that this chemistry is likely not limited to occurring on irradiated TiO_2 surfaces. The water catalyzed $NH_2 + O_2$ chemistry observed here likely occurs on other metal oxide surfaces that promote NH_2 formation via the dissociative chemisorption of NH_3 in several industrial applications. For example, ammonia activation and formation of NH_2 have been observed during thermal SCR of NO_x over vanadium- and tungsten-based oxide catalysts.[78,79] In addition, NH_2 is formed upon coadsorption of NH_3 and O_2 on RuO_2,[80] Pt,[81] and zeolite[82] surfaces, some of which have been investigated for oxidizing NH_3 to NO for use in industrial scale nitric acid production. The Ostwald process currently achieves this by oxidizing NH_3 in air over a Pt/Rh catalyst.[83,84] In the presence of O_2 and adsorbed water, chemisorption of NH_3 may also yield NO via the chemical pathways discussed here. In the environment other semiconducting metal oxides commonly found in urban areas (e.g., Fe_2O_3, Cr_2O_3, and ZnO) may also be capable of oxidizing NH_3 under certain conditions.[9,11,85] However, further research is needed to fully understand the role of water-catalyzed $NH_2 + O_2$ chemistry in other catalytic systems.

In urban environments NH_3 photooxidation will most likely occur on infrastructure with TiO_2 coatings (e.g., "self-cleaning" paint, glass, and concrete) that is exposed to vehicle emissions. To assess the atmospheric importance of this chemistry, we estimate the lifetime of NH_3 with respect to uptake on TiO_2 surfaces and compare this to the atmospheric lifetime of NH_3 due to gaseous dry deposition, which is one of the most important removal pathways of NH_3 from the troposphere.[86−88] The deposition velocity (υ_d) describing the loss of NH_3 to a TiO_2 surface may be estimated from $\upsilon_d = \gamma\omega/4$.[89] We assume the uptake coefficient (γ) for this process is ~3×10^{-5}, based on an ambient NH_3 concentration of 5 ppb at 48% RH (see Figure 2). To correct for differences in light intensity under experimental and outdoor conditions, we scale γ by the ratio of the actinic flux to the light intensity of our lamps. At an actinic flux[5] typical for the sun at a solar zenith angle of 0°, the uptake coefficient becomes 1.2×10^{-5}. Using this approach the υ_d is estimated to be 0.18 cm s^{-1}; this falls in the range of measured gaseous dry deposition velocities reported for NH_3 (i.e., 0.03−4 cm s^{-1}).[87,88] The lifetime (τ) with respect to NH_3 uptake on TiO_2 surfaces is calculated from $\tau = Z/\upsilon_d$, where Z is the boundary layer height. Assuming a 1 km high well-mixed boundary layer during the day, the lifetime of NH_3 with respect to loss on TiO_2 surfaces is 6 days. For comparison, reported dry deposition velocities[87,88] for NH_3 correspond to atmospheric lifetimes of between 7 h and 40 days. This suggests that photooxidation of ambient NH_3 on self-cleaning surfaces in urban areas is as effective as gaseous dry deposition in removing ammonia from ambient air.

Unlike dry deposition to nonreactive surfaces, our work shows that removal of NH_3 on irradiated TiO_2 surfaces is associated with the release of NO_x to air. The question remains how the proposed source of NO_x from NH_3 photooxidation compares to other urban sources of NO_x? Following the assumptions made above, the flux of NO_x from a TiO_2-coated surface is calculated from $Flux = \upsilon_d[NH_3]_{air}$ to be 2.2×10^{10} molecules cm^2 s^{-1}. The flux of NO_x from other urban surfaces is estimated by assuming steady-state conditions apply where the rate of NO_x production and loss are equal. The flux of NO_x from other sources is estimated from $Flux = Z[NO_x]/\tau_{NO_x}$, where τ_{NO_x} is the lifetime of NO_x in ambient air (i.e., 4 h at noon).[90] Assuming a noontime NO_x concentration of 1 ppb[5] and Z = 1 km, we estimate that a typical flux of NO_x is 1.7×10^{11} molecules cm^2 s^{-1}. Thus, the flux of NO_x from NH_3 photooxidation on TiO_2-coated surfaces is ~13% that of typical daytime sources of NO_x. This suggests that NH_3 photo-

dx.doi.org/10.1021/ja401846x | J. Am. Chem. Soc. 2013, 135, 8606−8615

oxidation could be important source of NO_x (and an indirect source of O_3) to air in the vicinity of TiO_2-coated structures.

AUTHOR INFORMATION

Corresponding Author

jdraff@indiana.edu; bgerber@uci.edu

Notes

The authors declare no competing financial interest.

ACKNOWLEDGMENTS

This work was funded by Indiana University, the National Science Foundation (grants CHE-0909227 and CHE-0840513), and the Israel Science Foundation (grant no. 172/12). We thank Prof. Philip Stevens for the use of the chemiluminescence NO_x analyzer. We also thank Prof. Sara Skrabalak for use of the surface area analysis system; Dr. Maren Pink for XRD analysis of the TiO_2 used in this study; Jörg Meyer and Donald Garvin for glassblowing; and Dr. János Szanyi (Pacific Northwest National Laboratory) for helpful discussions. We are grateful to the reviewers for their helpful comments.

REFERENCES

(1) Aneja, V. P.; Schlesinger, W. H.; Erisman, J. W. *Nat. Geosci.* **2008**, *1*, 409−411.

(2) Langford, A. O.; Fehsenfeld, F. C. *Science* **1992**, *255*, 581−583.

(3) Fraser, M. P.; Cass, G. R. *Environ. Sci. Technol.* **1998**, *32*, 1053−1057.

(4) Biermann, H. W.; Tuazon, E. C.; Winer, A. M.; Wallington, T. J.; Pitts, J. N. *Atmos. Environ.* **1988**, *22*, 1545−1554.

(5) Finlayson-Pitts, B. J.; Pitts, J. N., Jr. *Chemistry of the Upper and Lower Atmosphere - Theory, Experiments, and Applications*; Academic Press: San Diego, 2000.

(6) Sander, S. P.; Finlayson-Pitts, B. J.; Friedl, R. R.; Golden, D. M.; Huie, R. E.; Keller-Rudek, H.; Kolb, C. E.; Kurylo, M. J.; Molina, M. J.; Moortgat, G. K.; Orkin, V. L.; Ravishankara, A. R.; Wine, P. H. *Chemical Kinetics and Photochemical Data for Use in Atmospheric Studies, Evaluation Number 15, JPL Publication 06−2*; Jet Propulsion Laboratory: Pasadena, 2006.

(7) Hughes, L. S.; Allen, J. O.; Bhave, P.; Kleeman, M. J.; Cass, G. R.; Liu, D. Y.; Fergenson, D. P.; Morrical, B. D.; Prather, K. A. *Environ. Sci. Technol.* **2000**, *34*, 3058−3068.

(8) Seinfeld, J. H.; Pandis, S. N. *Atmospheric chemistry and physics: from air pollution to climate change*; 2nd ed.; John Wiley & Sons, Inc.: Hoboken, 2006.

(9) Usher, C. R.; Michel, A. E.; Grassian, V. H. *Chem. Rev.* **2003**, *103*, 4883−4940.

(10) Dubowski, Y.; Sumner, A. L.; Menke, E. J.; Gaspar, D. J.; Newberg, J. T.; Hoffman, R. C.; Penner, R. M.; Hemminger, J. C.; Finlayson-Pitts, B. J. *Phys. Chem. Chem. Phys.* **2004**, *6*, 3879−3888.

(11) Chen, H.; Nanayakkara, C. E.; Grassian, V. H. *Chem. Rev.* **2012**, *112*, 5919−5948.

(12) Hoffmann, M. R.; Martin, S. T.; Choi, W.; Bahnemann, D. W. *Chem. Rev.* **1995**, *95*, 69−96.

(13) Pope, F. D.; Braesicke, P.; Grainger, R. G.; Kalberer, M.; Watson, I. M.; Davidson, P. J.; Cox, R. A. *Nat. Clim. Change* **2012**, *2*, 713−719.

(14) Guarino, M.; Costa, A.; Porro, M. *Bioresour. Technol.* **2008**, *99*, 2650−2658.

(15) Abdullah, H. Z.; Taib, H.; Sorrell, C. C. *Adv. Appl. Ceram.* **2007**, *106*, 105−112.

(16) Dockery, D. W.; Pope, C. A.; Xu, X.; Spengler, J. D.; Ware, J. H.; Fay, M. E.; Ferris, B. G.; Speizer, F. E. *New Engl. J. Med.* **1993**, *329*, 1753−1759.

(17) Gauderman, W. J.; Avol, E.; Gilliland, F.; Vora, H.; Thomas, D.; Berhane, K.; McConnell, R.; Kuenzli, N.; Lurmann, F.; Rappaport, E.; Margolis, H.; Bates, D.; Peters, J. *New Engl. J. Med.* **2004**, *351*, 1057−1067.

(18) Gustafsson, R. J.; Orlov, A.; Griffiths Paul, T.; Cox, R. A.; Lambert Richard, M. *Chem. Commun.* **2006**, *37*, 3936−3938.

(19) Stemmler, K.; Ammann, M.; Donders, C.; Kleffmann, J.; George, C. *Nature* **2006**, *440*, 195−198.

(20) Ndour, M.; Conchon, P.; D'Anna, B.; Ka, O.; George, C. *Geophys. Res. Lett.* **2009**, *36*, L05816.

(21) Monge, M. E.; D'Anna, B.; George, C. *Phys. Chem. Chem. Phys.* **2010**, *12*, 8991−8998.

(22) Monge, M. E.; D'Anna, B.; Mazri, L.; Giroir-Fendler, A.; Ammann, M.; Donaldson, D. J.; George, C. *Proc. Natl. Acad. Sci. U.S.A.* **2010**, *107*, 6605−6609.

(23) Laufs, S.; Burgeth, G.; Duttlinger, W.; Kurtenbach, R.; Maban, M.; Thomas, C.; Wiesen, P.; Kleffmann, J. *Atmos. Environ.* **2010**, *44*, 2341−2349.

(24) McLean, W. R.; Ritchie, M. *J. Appl. Chem.* **1965**, *15*, 452−460.

(25) Chuang, C.-C.; Shiu, J.-S.; Lin, J.-L. *Phys. Chem. Chem. Phys.* **2000**, *2*, 2629−2633.

(26) Tanaka, T.; Teramura, K.; Arakaki, K.; Funabiki, T.; Photoassisted, N. O. *Chem. Commun.* **2002**, *22*, 2742−2743.

(27) Yamazoe, S.; Okumura, T.; Hitomi, Y.; Shishido, T.; Tanaka, T. *J. Phys. Chem. C* **2007**, *111*, 11077−11085.

(28) Yamazoe, S.; Teramura, K.; Hitomi, Y.; Shishido, T.; Tanaka, T. *J. Phys. Chem. C* **2007**, *111*, 14189−14197.

(29) Koebel, M.; Elsener, M.; Madia, G. *Ind. Eng. Chem. Res.* **2000**, *40*, 52−59.

(30) Busca, G.; Lietti, L.; Ramis, G.; Berti, F. *Appl. Catal., B* **1998**, *18*, 1−36.

(31) Brandenberger, S.; Kröcher, O.; Tissler, A.; Althoff, R. *Catal. Rev.* **2008**, *50*, 492−531.

(32) Yamazoe, S.; Okumura, T.; Teramura, K.; Tanaka, T. *Catal. Today* **2006**, *111*, 266−270.

(33) George, C.; Strekowski, R. S.; Kleffmann, J.; Stemmler, K.; Ammann, M. *Farad. Discuss.* **2005**, *130*, 195−210.

(34) Thornberry, T.; Abbatt, J. P. D. *Phys. Chem. Chem. Phys.* **2003**, *6*, 84−93.

(35) Leu, M.-T.; Timonen, R. S.; Keyser, L. F.; Yung, Y. L. *J. Phys. Chem.* **1995**, *99*, 13203−13212.

(36) Kraus, A.; Rohrer, F.; Hofzumahaus, A. *Geophys. Res. Lett.* **2000**, *27*, 1115−1118.

(37) Crowley, J. N.; Ammann, M.; Cox, R. A.; Hynes, R. G.; Jenkin, M. E.; Mellouki, A.; Rossi, M. J.; Troe, J.; Wallington, T. J. *Atmos. Chem. Phys.* **2010**, *10*, 9059−9223.

(38) Stemmler, K.; Ndour, M.; Elshorbany, Y.; Kleffmann, J.; D'Anna, B.; George, C.; Bohn, B.; Ammann, M. *Atmos. Chem. Phys.* **2007**, *7*, 4237−4248.

(39) Murphy, D. M.; Fahey, D. W. *Anal. Chem.* **1987**, *59*, 2753−2759.

(40) Behnke, W.; George, C.; Scheer, V.; Zetzsch, C. *J. Geophys. Res.* **1997**, *102*, 3795−3804.

(41) Ghiaasiaan, S. M. *Two-Phase Flow, Boiling, and Condensation In Conventional and Miniature Systems*; Cambridge University Press: New York, 2007.

(42) Nicolas, M.; Ndour, M.; Ka, O.; D'Anna, B.; George, C. *Environ. Sci. Technol.* **2009**, *43*, 7437−7442.

(43) Njegic, B.; Raff, J. D.; Finlayson-Pitts, B. J.; Gordon, M. S.; Gerber, R. B. *J. Phys. Chem. A* **2010**, *114*, 4609−4618.

(44) Weigend, F.; Häser, M. *Theor. Chem. Acc.* **1997**, *97*, 331−340.

(45) Dunning, T. H., Jr. *J. Chem. Phys.* **1989**, *90*, 1007−1023.

(46) Kendall, R. A.; Dunning, T. H.; Harrison, R. J. *J. Chem. Phys.* **1992**, *96*, 6796−6806.

(47) Stanton, J. F. *J. Chem. Phys.* **1994**, *101*, 371−374.

(48) Reed, A. E.; Weinstock, R. B.; Weinhold, F. *J. Chem. Phys.* **1985**, *83*, 735−746.

(49) Raghavachari, K.; Trucks, G. W.; Pople, J. A.; Head-Gordon, M. *Chem. Phys. Lett.* **1989**, *157*, 479−483.

(50) Weigend, F.; Häser, M.; Patzelt, H.; Ahlrichs, R. *Chem. Phy. Lett.* **1998**, *294*, 143−152.

(51) *TURBOMOLE*, V6.3 2011, a development ofUniversity of Karlsruhe and Forschungszentrum Karlsruhe GmbH, 1989−2007, TURBOMOLE GmbH, since 2007; http://www.turbomole.com.
(52) Ohtani, B.; Prieto-Mahaney, O. O.; Li, D.; Abe, R. *Photochem. Photobiol. A* **2010**, *216*, 179−182.
(53) Agrios, A. G.; Pichat, P. *J. Appl. Electrochem.* **2005**, *35*, 655−663.
(54) Agrios, A. G.; Gray, K. A. *Environ. Catal.* **2005**, 369−390.
(55) Kwon, S.; Fan, M.; Cooper, A. T.; Yang, H. *Crit. Rev. Environ. Sci Technol.* **2008**, *38*, 197−226.
(56) Hurum, D. C.; Agrios, A. G.; Gray, K. A.; Rajh, T.; Thurnauer, M. C. *J. Phys. Chem. B* **2003**, *107*, 4545−4549.
(57) Ndour, M.; D'Anna, B.; George, C.; Oumar, K.; Balkanski, Y.; Kleffmann, J.; Stemmler, K.; Ammann, M. *Geophys. Res. Lett.* **2008**, *35*, L05812.
(58) Hadjiivanov, K.; Lamotte, J.; Lavalley, J.-C. *Langmuir* **1997**, *13*, 3374−3381.
(59) Socrates, G. *Infrared and Raman Characteristic Group Frequencies*; John Wiley & Sons: Chichester, 2001.
(60) Donaldson, D. J. *J. Phys. Chem. A* **1998**, *103*, 62−70.
(61) Lee, C.; Fitzgerald, G.; Planas, M.; Novoa, J. J. *J. Phys. Chem.* **1996**, *100*, 7398−7404.
(62) Roberts, S. T.; Petersen, P. B.; Ramasesha, K.; Tokmakoff, A.; Ufimtsev, I. S.; Martinez, T. J. *Proc. Natl. Acad. Sci. U.S.A.* **2009**, *106*, 15154−15159.
(63) Xantheas, S. S. *J. Am. Chem. Soc.* **1995**, *117*, 10373−10380.
(64) Szczepankiewicz, S. H.; Colussi, A. J.; Hoffmann, M. R. *J. Phys. Chem. B* **2000**, *104*, 9842−9850.
(65) Neta, P.; Maruthamuthu, P.; Carton, P. M.; Fessenden, R. W. *J. Phys. Chem.* **1978**, *82*, 1875−1878.
(66) Zhu, X.; Castleberry, S. R.; Nanny, M. A.; Butler, E. C. *Environ. Sci. Technol.* **2005**, *39*, 3784−3791.
(67) Kapałka, A.; Joss, L.; Anglada, Á.; Comninellis, C.; Udert, K. M. *Electrochem. Commun.* **2010**, *12*, 1714−1717.
(68) Kapałka, A.; Fierro, S.; Frontistis, Z.; Katsaounis, A.; Neodo, S.; Frey, O.; de Rooij, N.; Udert, K. M.; Comninellis, C. *Electrochim. Acta* **2011**, *56*, 1361−1365.
(69) Laszlo, B.; Alfassi, Z. B.; Neta, P.; Huie, R. E. *J. Phys. Chem. A* **1998**, *102*, 8498−8504.
(70) Hadjiivanov, K.; Knozinger, H. *Phys. Chem. Chem. Phys.* **2000**, *2*, 2803−2806.
(71) Volodin, A. M.; Malykhin, S. E.; Zhidomirov, G. M. *Kinet. Catal.* **2011**, *52*, 605−619.
(72) Sing, K. S. W.; Everett, D. H.; Haul, R. A. W.; Moscou, L.; Pierotti, R. A.; Rouquérol, J.; Siemieniewska, T. *Pure Appl. Chem.* **1985**, *57*, 603−619.
(73) Grünberg, B.; Emmler, T.; Gedat, E.; Shenderovich, I.; Findenegg, G. H.; Limbach, H.-H.; Buntkowsky, G. *Chem.−Eur. J.* **2004**, *10*, 5689−5696.
(74) Solveyra, E. G.; Llave, E. d. l.; Molinero, V.; Soler-Illia, G. J. A. A.; Scherlis, D. A. *J. Phys. Chem. C* **2013**, *117*, 3330−3342.
(75) Sumathi, R.; Peyerimhoff, S. D. *J. Chem. Phys.* **1998**, *108*, 5510−5521.
(76) Odenbrand, C. U. I.; Gabrielsson, P. L. T.; Brandin, J. G. M.; Andersson, L. A. H. *Appl. Catal.* **1991**, *78*, 109−122.
(77) Topsøe, N.-Y.; Slabiak, T.; Clausen, B. S.; Srnak, T. Z.; Dumesic, J. A. *J. Catal.* **1992**, *134*, 742−746.
(78) Ramis, G.; Larrubia, M. A.; Busca, G. *Top. Catal.* **2000**, *11/12*, 161−166.
(79) Ramis, G.; Yi, L.; Busca, G. *Catal. Today* **1996**, *28*, 373−380.
(80) Wang, Y.; Jacobi, K.; Schöne, W. D.; Ertl, G. *J. Phys. Chem. B* **2005**, *109*, 7883−7893.
(81) Offermans, W. K.; Jansen, A. P. J.; van Santen, R. A.; Novell-Leruth, G.; Ricart, J. M.; Perez-Ramirez, J. *J. Phys. Chem. C* **2007**, *111*, 17551−17557.
(82) Hashimoto, K.; Toukai, N. *J. Mol. Catal. A: Chem.* **2000**, *161*, 171−178.
(83) Wagner, E.; Fetzer, T. In *Handbook of heterogeneous catalysis*; Ertl, G., Knozinger, H., Weitkamp, J., Eds.; Wiley-VCH: New York, 1997; Vol. *4*, p 1748.
(84) Schlögl, R. *Angew. Chem., Int. Ed.* **2003**, *42*, 2004−2008.
(85) Nishino, N.; Finlayson-Pitts, B. J. *Phys. Chem. Chem. Phys.* **2012**, *14*, 15840−15848.
(86) Smith, A. M.; Keene, W. C.; Maben, J. R.; Pszenny, A. A. P.; Fischer, E.; Stohl, A. *J. Geophys. Res.: Atmos.* **2007**, *112*, D10S08.
(87) Phillips, S. B.; Arya, S. P.; Aneja, V. P. *Atmos. Environ.* **2004**, *38*, 3469−3480.
(88) Zbieranowski, A. L.; Aherne, J. *Atmos. Environ.* **2012**, *62*, 481−491.
(89) Dentener, F. J.; Carmichael, G. R.; Zhang, Y.; Lelieveld, J.; Crutzen, P. J. *J. Geophys. Res.* **1996**, *101*, 22869−22889.
(90) Beirle, S.; Boersma, K. F.; Platt, U.; Lawrence, M. G.; Wagner, T. *Science* **2011**, *333*, 1737−1739.